

Novel Method for Detection of Genes With Altered Expression Caused by Coronavirus Infection and Screening of Candidate Drugs for SARS-CoV-2

Y-H. Taguchi and Turki Turki

Abstract—To better understand the genes with altered expression caused by infection with the novel coronavirus strain SARS-CoV-2 causing COVID-19 infectious disease, a tensor decomposition (TD)-based unsupervised feature extraction (FE) approach was applied to a gene expression profile dataset of the mouse liver and spleen with experimental infection of mouse hepatitis virus, which is regarded as a suitable model of human coronavirus infection. TD-based unsupervised FE selected 134 altered genes, which were enriched in protein-protein interactions with orf1ab, polyprotein, and 3C-like protease that are well known to play critical roles in coronavirus infection, suggesting that these 134 genes can represent the coronavirus infectious process. We then selected compounds targeting the expression of the 134 selected genes based on a public domain database. The identified drug compounds were mainly related to known antiviral drugs, several of which were also included in those previously screened with an *in silico* method to identify candidate drugs for treating COVID-19.

Index Terms—COVID-19, SARS-CoV-2, *in silico* drug discovery, gene expression profile, tensor decomposition, feature extraction

I. INTRODUCTION

THE current pandemic of COVID-19 caused by infection of the new coronavirus strain SARS-CoV-2 is a severe public health problem that must be resolved as soon as possible. To achieve this goal, it is essential to understand the mechanism by which SARS-CoV-2 successfully invades human cells. Recently, Pfaender et al. [1] demonstrated that host lymphocyte antigen 6 (LY6E) complex impairs coronavirus fusion and confers immune control of viral disease. The authors also used a transcriptome approach to evaluate the effect of infection of mouse hepatitis virus (MHV), a natural mouse pathogen that causes hepatitis and encephalomyelitis, which is a well-studied model of coronavirus infection. Although they found many pathways that were disturbed after MHV infection, they did not perform a detailed analysis of the genes with altered expression in response to MHV infection.

In this study, we applied tensor decomposition (TD)-based unsupervised feature extraction (FE) [2] to identify genes with altered expression by MHV infection as a model of coronavirus. We further performed functional enrichment on the selected genes to determine their potential associations

with coronavirus infection processes, and screened candidate drug compounds targeting these genes. Overall, this work expands TD formalism by exploring the interpretation of six-dimensional tensors in an infectious disease context. Moreover, we demonstrate a novel application of TD to facilitate the drug discovery process, which can offer a valuable resource for researchers to obtain mechanistic insight for identifying effective drugs for infectious diseases such as COVID-19.

II. MATERIALS AND METHODS

A. Gene expression profile dataset

The gene expression profile was downloaded from the Gene Expression Omnibus (GEO) dataset GSE146074. This dataset comprises the gene expression profiles of the liver and spleen from female mice experimentally infected with MHV or injected with phosphate-buffered saline (PBS) as a control group for comparison. This experiment was performed with mice of two genetic backgrounds, including wild-type (WT) mice and an *textit{Ly6e}*-knockout (KO) mutant strain. The number of replicates for each group are listed in Table I. Seventy two files whose names start by “GSM” (processed file) were used for analyses.

TABLE I
NUMBER OF BIOLOGICAL REPLICATES. TWO TECHNICAL REPLICATES ARE AVAILABLE FOR EACH BIOLOGICAL REPLICATE.

	PBS day 5		MHV day 3		MHV day 5	
	liver	spleen	liver	spleen	liver	spleen
WT	3	3	3	3	3	3
KO	3	3	3	3	3	3

B. Additional gene expression profile data set

In order to validate the suitability of MHV as model SARS-CoV-2 infectious process, two additional gene expression profiles of mice lung SARS-CoV infectious processes (Table II. For GSE33266 and GSE50000, we download two files *GSE33266_series_matrix.txt.gz* and *GSE50000_series_matrix.txt.gz*, respectively. Although GSE50000 also includes files for SARS-CoV-MA15, they were omitted (the reason why we did not use files for MA15 can be available at Discussion section). For the cases that have less than five biological replicates, we used more than once some of replicates in order to have five biological replicates for individual cases.

Y-H. Taguchi is with the Department of Physics, Chuo University, Tokyo 112-8551, Japan, e-mail:tag@granular.com (see https://researchmap.jp/Yh_Taguchi/).

Turki Turki is with the Department of Computer Science, King Abdulaziz University, Jeddah 21589, Saudi Arabia

TABLE II
NUMBER OF BIOLOGICAL REPLICATES OF SARS-CoV INFECTION
TOWARD MOUSE LUNG GENE EXPRESSION PROFILES

GSE33266				
days	D1	D2	D4	D7
Mock	3	3	3	3
10 ² pfu	5	5	5	5
10 ³ pfu	5	5	5	5
10 ⁴ pfu	5	5	5	5
10 ⁵ pfu	5	5	5	5
GSE50000				
days	d1	d2	d4	d7
BatSRBD	5	5	5	4
icSARS	4	5	5	5
Mock	4	4	4	4

C. TD-based unsupervised FE

Figure 1 shows the flowchart of TD based unsupervised FE.

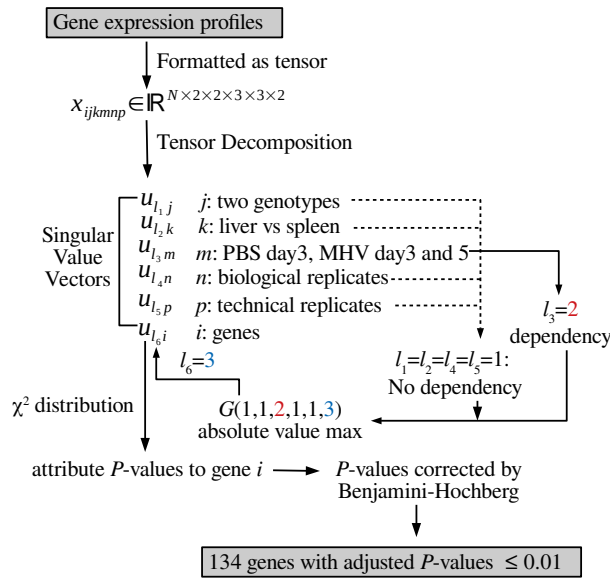


Fig. 1. Flow chart of TD based unsupervised FE

The gene expression profile dataset was formatted as a tensor, $x_{ijkmp} \in \mathbb{R}^{N \times 2 \times 2 \times 3 \times 3 \times 2}$, which represents the expression level of the i th gene of the j th genotype ($j = 1$:KO, $j = 2$:WT) of the k th tissue ($k = 1$:liver, $k = 2$:spleen) of the m th treatment group ($m = 1$:PBS day 5, $m = 2$:MHV day 3, $m = 3$:MHV day 5) for the n th biological replicate ($1 \leq n \leq 3$) and p th technical replicate ($1 \leq p \leq 2$).

The TD is therefore expressed as

$$x_{ijkmp} = \sum_{l_1 l_2 l_3 l_4 l_5 l_6} G(l_1 l_2 l_3 l_4 l_5 l_6) \times u_{l_1 j} u_{l_2 k} u_{l_3 m} u_{l_4 n} u_{l_5 p} u_{l_6 i} \quad (1)$$

where $G(l_1 l_2 l_3 l_4 l_5 l_6) \in \mathbb{R}^{N \times 2 \times 2 \times 3 \times 3 \times 2}$ is a core tensor, and $u_{l_1 j} \in \mathbb{R}^{2 \times 2}$, $u_{l_2 k} \in \mathbb{R}^{2 \times 2}$, $u_{l_3 m} \in \mathbb{R}^{3 \times 3}$, $u_{l_4 n} \in \mathbb{R}^{3 \times 3}$, $u_{l_5 p} \in \mathbb{R}^{2 \times 2}$, and $u_{l_6 i} \in \mathbb{R}^{N \times N}$ are singular values vectors, which can be obtained via the higher-order singular value decomposition (HOSVD) algorithm [2].

To select $u_{l_6 i}$, attributed to selected genes, we need to select $u_{l_1 j}$ attributed to the genotype, $u_{l_2 k}$ attributed to the

tissue, $u_{l_3 m}$ attributed to the treatment, $u_{l_4 n}$ attributed to the biological replicate, and $u_{l_5 p}$ attributed to the technical replicate, associated with desired properties.

For this study, we sought to identify genes whose expression is independent of the mouse genotype, tissue type, and replicate. Thus, $u_{l_1 j}$, $u_{l_2 k}$, $u_{l_4 n}$, and $u_{l_5 p}$ should be independent of j , k , n , and p .

By contrast, we require $u_{l_3 m}$ to be dependent on $u_{l_3 1} < u_{l_3 2} < u_{l_3 3}$ or vice versa. This is because $m = 2$ (3 days after MHV infection) must be between $m = 1$ (5 days after PBS injection as the control) and $m = 3$ (5 days after MHV infection).

After selecting l_1, l_2, l_3, l_4 , and l_5 based on the above considerations, we selected l_6 associated with $G(l_1 l_2 l_3 l_4 l_5 l_6)$ as the largest absolute value, with fixed l_1, l_2, l_3, l_4 , and l_5 values. Using the selected $u_{l_6 i}$, The P -values, P_i s, were attributed to gene expression levels as

$$P_i = P_{\chi^2} \left[> \left(\frac{u_{l_6 i}}{\sigma_{l_6}} \right)^2 \right] \quad (2)$$

where $P_{\chi^2}[> x]$ is the cumulative probability distribution of the χ^2 distribution when the argument is larger than x and σ_{l_6} is the standard deviation of $u_{l_6 i}$.

P_i s were adjusted by the Benjamini and Hochberg (BH) criterion [2], and only genes associated with an adjusted P_i less than 0.01 were selected for further analysis.

We employed the almost same procedures excluding different structure of tensors analyses toward two additional gene expression profiles of mice lung SARS-CoV infectious processes. The tensors formatted and TDs are for GSE33266

$$x_{ijkn} \in \mathbb{R}^{N \times 5 \times 4 \times 5} \quad (3)$$

$$= \sum_{l_1=1}^5 \sum_{l_2=1}^4 \sum_{l_3=1}^5 \sum_{l_4=1}^N G(l_1 l_2 l_3 l_4) \times u_{l_1 j} u_{l_2 k} u_{l_3 n} u_{l_4 i} \quad (4)$$

which represents i th gene expression profile of j th experiments ($j = 1$:Mock, $j = 2$:10²pfu, $j = 3$:10³pfu, $j = 4$:10⁴pfu, $j = 5$:10⁵pfu) at k th day after infection ($k = 1$:D1, day 1, $k = 2$:D2, day 2, $k = 3$:D4, day 4, $k = 4$:D7, day 7) of n th biological replicates ($1 \leq n \leq 5$). $G(l_1 l_2 l_3 l_4) \in \mathbb{R}^{N \times 5 \times 4 \times 5}$ is a core tensor that represents the weight of products of singular value matrices, $u_{l_1 j} \in \mathbb{R}^{5 \times 5}$, $u_{l_2 k} \in \mathbb{R}^{4 \times 4}$, $u_{l_3 n} \in \mathbb{R}^{5 \times 5}$, and $u_{l_4 i} \in \mathbb{R}^{N \times N}$ which are all orthogonal matrices. Those for GSE50000 are

$$x_{ijkn} \in \mathbb{R}^{N \times 3 \times 4 \times 5} \quad (5)$$

$$= \sum_{l_1=1}^5 \sum_{l_2=1}^4 \sum_{l_3=1}^5 \sum_{l_4=1}^N G(l_1 l_2 l_3 l_4) \times u_{l_1 j} u_{l_2 k} u_{l_3 n} u_{l_4 i} \quad (6)$$

which represents i th gene expression profile of j th experiments ($j = 1$:BatSRBD, $j = 2$:icSARS, $j = 3$:Mock) at k th day after infection ($k = 1$:d1, day 1, $k = 2$:d2, day 2, $k = 3$:d4, day 4, $k = 4$:d7, day 7) of n th biological replicates ($1 \leq n \leq 5$). $G(l_1 l_2 l_3 l_4) \in \mathbb{R}^{N \times 3 \times 4 \times 5}$ is a core tensor that represents the weight of products of singular value matrices,

$u_{\ell_1 j} \in \mathbb{R}^{3 \times 3}$, $u_{\ell_2 k} \in \mathbb{R}^{4 \times 4}$, $u_{\ell_3 n} \in \mathbb{R}^{5 \times 5}$, and $u_{\ell_4 i} \in \mathbb{R}^{N \times N}$ which are all orthogonal matrices.

The criteria for the selections of singular value vectors are as follows. For GSE33266, $u_{\ell_1 j}$ should be monotonic function of j , since it represents the strength of infection, $u_{\ell_2 k}$ also should be monotonic function of k , since it is time development, and $u_{\ell_3 n}$ should be constant since biological replicates should not differ from one another. For GSE50000, $u_{\ell_1 j}$ should be distinct between $k = 3$ and $k = 1, 2$, since it represents the distinction between Mock and infection, $u_{\ell_2 k}$ also should be monotonic function of k , since it is time development, and $u_{\ell_3 n}$ should be constant since biological replicates should not differ from one another.

Downstream procedures for gene selection after identifying singular value vectors are the same as those for MHV. Core tensors, $G(\ell_1 \ell_2 \ell_3 \ell_4)$ s, are investigated in order to see which ℓ_4 associated with $G(\ell_1 \ell_2 \ell_3 \ell_4)$ having larger absolute values given ℓ_1, ℓ_2, ℓ_3 . $u_{\ell_4 i}$ s selected are used for attributing P -values, P_i , to genes and genes associated with adjusted P -values less than 0.01 were selected.

D. Enrichment analysis

Gene symbols of genes selected by TD-based unsupervised FE with significantly altered expression due to MHV infection were uploaded to Enricher [3] and Metascape [4], which are popular enrichment analysis servers that evaluate the biological properties of genes based on enrichment analysis.

III. RESULTS

Figure 2 shows the overview of analyses performed in this study.

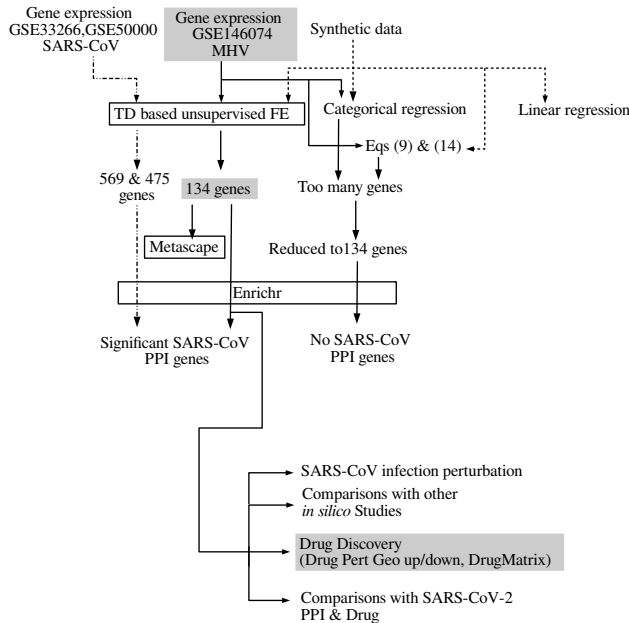


Fig. 2. Overview of analyses

A. Synthetic data sets

In order to demonstrate how effective tensor is, we employ synthetic data sets composed of multiway and multiclass labels, $x_{ijk s} \in \mathbb{R}^{N \times M \times K \times S}$. Here, i represents N variables, among which partial collections having distinct values between j s as well as k s must be selected where S replicates are available for individual combinations of j and k . A typical example is that $x_{ijk s}$ represents expression of i th genes in k th tissue of patients who belong to j th group that consists of S patients. Then the purpose is to identify which genes are expressed distinctly in the tissue (k)-specific as well as patients group (j) specific ways.

The most popular approach to address this problem is linear regression,

$$x_{ijk s} = \alpha_i a_j + \beta_i b_k + \gamma_i \quad (7)$$

where a_j and b_k are the pre-defined variables that represent some properties of j th patients group and k th tissue, respectively. $\alpha_i, \beta_i, \gamma_i$ are regression coefficients that are supposed to be selected such that the discrepancy between both sides of equation is minimized. Then i s associated with significant P -values are selected as those whose expression are distinct between distinct j s and k s, respectively.

Of course, it is not guaranteed that liner regression correctly figure out the dependency of $x_{ijk s}$ upon j and k . Here we generate synthetic data that follows

$$x_{ijk s} = \xi_{ijk} a_j b_k + \varepsilon_{ijk s} \quad (8)$$

where ξ_{ijk} are drawn from $\mathcal{N}(1, 0)$ for every combination of i, j, k (this means that $x_{ijk s}$ s associated with distinct s s share the same ξ_{ijk}) and $\varepsilon_{ijk s}$ are drawn from $\mathcal{N}(1, 0)$ for every combination of i, j, k, s . $\mathcal{N}(\mu, \sigma)$ represents the normal distribution that has mean of μ and standard deviation of σ . For $i \geq N_0$, α_{ijk} is taken to be zero; this means that $x_{ijk s}$ for $i \geq N_0$ is simply random variables. The task is to correctly select N_0 variables associated with the dependence upon j and k .

As an alternative regression analysis of liner regression, we employ

$$x_{ijk} = \alpha'_i a_j b_k + \gamma'_i \quad (9)$$

which reflects the multiplicative nature when x_{ijk} is generated with eq. (8) although it cannot represent x_{ijk} completely since α_{ijk} is replaced with α_i (i.e., dependence upon j or k is not assumed).

In addition to the above two regression analysis, we also applied categorical regression that is known to be equivalent to analysis of variance (ANOVA)

$$x_{ijk s} = \sum_{j'=1}^M \sum_{k'=1}^K \alpha_{ij'k'} \delta_{jj'} \delta_{kk'} + \gamma''_i \quad (10)$$

where $\delta_{jj'}$ and $\delta_{kk'}$ are Kronecker's delta and $\alpha_{ij'k'}$ and γ''_i are regression coefficients, respectively. One should notice that eq. (10) can fully reproduce x_{ijk} generated by eq. (8), when $\alpha_{ij'k'}$ is taken to be $\xi_{ij'k'} a_{j'} b_{k'}$ excluding randomness introduced by $\varepsilon_{ijk s}$, which can be regarded as residuals.

TABLE III

THE CONFUSION MATRICES OBTAINED USING SYNTHETIC DATA (EQ.(8), $N = 1000, N_0 = 100, M = K = 3, S = 5$) AND CPU TIME REQUIRED FOR EACH METHOD. P_s ARE THRESHOLD P -VALUES; i ASSOCIATED WITH ADJUSTED P -VALES LESS THAN THIS THRESHOLD VALUES ARE SELECTED.

P	0.01		0.1	
TD based unsupervised FE (eq. (11), cpu time 6.5 sec)				
	not selected	selected	not selected	selected
$i > N_0$	900	62.2	899.9	48.44
$i \leq N_0$	0	37.8	0.1	51.56
linar regression (eq. (7), cpu time 65.7 sec)				
	not selected	selected	not selected	selected
$i > N_0$	899.7	75.39	894.0	58.31
$i \leq N_0$	0.3	24.61	6.0	41.69
categorical regression (70.4 sec)				
	not selected	selected	not selected	selected
$i > N_0$	897.3	0	—	—
$i \leq N_0$	2.7	100	—	—
eq. (9) (84.1 sec)				
	not selected	selected	not selected	selected
$i > N_0$	900	84.55	899.3	74.0
$i \leq N_0$	0	14.55	0.7	26.0

Finally, we also applied TD based unsupervised FE to x_{ijks} . TD is computed as

$$x_{ijks} = \sum_{\ell_4=1}^N \sum_{\ell_1=1}^M \sum_{\ell_2=1}^K \sum_{\ell_3=1}^S G(\ell_1 \ell_2 \ell_3 \ell_4) u_{\ell_1 j} u_{\ell_2 k} u_{\ell_3 s} u_{\ell_4 i} \quad (11)$$

Then ℓ_1 and ℓ_2 that have largest absolute values of correlation coefficients between $u_{\ell_1 j}$ and a_j or $u_{\ell_2 k}$ and b_k are selected. Then top two ℓ_1 that have larger absolute $G(\ell_1 \ell_2 1 \ell_4)$ s are selected. The reason why ℓ_3 is fixed to be 1 is because u_{1s} always represent $u_{\ell_3 s}$ that lacks s dependency, i.e., constant independent of s (Since x_{ijks} should take same values between replicates, $u_{\ell_3 s}$ that do not have any s dependence is selected). Then P -values are attributed to i as

$$P_i = P_{\chi^2} \left[> \sum_{\ell_4} \left(\frac{u_{\ell_4 i}}{\sigma_{\ell_4}} \right)^2 \right] \quad (12)$$

where summation is taken over two selected ℓ_4 only.

No matter which one of liner regression (eq.(7)), eq. (9), categorical regression (eq.(10)) or TD (eq.(11)) is used to compute P_i , P_i is corrected by BH criterion [2] and i s having corrected P_i less than threshold P -values are selected as those associated with dependency upon j and k , respectively.

For simplicity, we employ $a_j = j$ and $b_k = k$ when generating x_{ijks} using eq. (8) as well as eq. (9) is used for regression analysis. Specifically, we chose $N = 1000, N_0 = 100, M = K = 3, S = 5$. Generation of x_{ijks} and selection of i s are repeated by 100 times with two distinct threshold P -values 0.01 or 0.1 for each trial. Table III shows the averaged performance over 100 trials. Although categorical regression, eq. (10), can outperform other three since it is expected to completely reproduce eq. (8) as denoted in the above, it has one weak point; it cannot explicitly consider the dependence of a_j and b_k upon j and k , since $\xi_{ijk} a_j b_k$ s are estimated as one parameter α_{ijk} . This might prevent us from selecting i s that are specifically associated with the dependence upon j and k that a_j and b_k represent. Even if some i s are selected,

TABLE IV

$G(1, 1, 2, 1, 1, \ell_6)$ S COMPUTED BY THE HOSVD ALGORITHM

ℓ_6	$G(1, 1, 2, 1, 1, \ell_6)$	ℓ_6	$G(1, 1, 2, 1, 1, \ell_6)$
1	-11.846381	6	22.375546
2	-28.104674	7	-41.997092
3	312.362569	8	-9.048416
4	-71.001444	9	9.212773
5	-189.719321	10	3.394629

it might because of dependence upon j and k that a_j and b_k do not represent. There are no ways for us to check this point. In this sense, TD based unsupervised FE, which is the second best, is better than categorical regression since TD based unsupervised FE can consider a_j and b_k when selecting $u_{\ell_1 j}$ and $u_{\ell_2 k}$ correlated with a_j and b_k , respectively.

Another advantages of TD based unsupervised FE is short cpu time required (Table III). Roughly speaking, cpu time required for TD based unsupervised FE is one tenth of other three methods that must repeat regression analysis by N times. This difference might matter when we are forced to deal with massive data set.

The reason why TD based unsupervised FE can consider dependence upon j and k that a_j and b_k have although other methods cannot is as follows; because of random nature of ξ_{ijk} in eq. (8), when individual i is considered, there are no ways to consider dependence upon j and k that a_j and b_k have. Nevertheless, when x_{ijks} s are averaged over multiple i s, there are some possibilities that dependence upon j and k that a_j and b_k have can appear, since randomness of ξ_{ijk} can be smeared out because of averaging. In actual, since $u_{\ell_1 j}$ as well as $u_{\ell_2 k}$ can be such variables that can appear only after averaging and can represent dependence upon j and k that a_j and b_k have. This is the reason why TD based unsupervised FE can outperform eq. (9) that explicitly consider multiplicative nature when x_{ijks} s are generated and can consider dependence upon j and k that a_j and b_k have, which categorical regression, eq.(10), cannot.

B. Selection of genes

At first, we apply TD based unsupervised FE to gene expression profiles introduced in Materials and Methods. Then other methods applied to synthetic data set than TD based unsupervised FE are considered for the comparisons in the next section, discussions and conclusions.

We selected $\ell_1 = 1, \ell_2 = 1, \ell_3 = 2, \ell_4 = 1$, and $\ell_5 = 1$ based on the criteria described above (Fig. 3), and the associated $G(1, 1, 2, 1, 1, \ell_6)$ values are listed in Table IV, demonstrating the largest value for $G(1, 1, 2, 1, 1, 3)$. The associated P_i values were computed using u_{3i} as shown in eq. (2), resulting in selection of 134 genes altered in MHV infection with adjusted P -values less than 0.01 (Table V). Although some mouse-specific genes were included in this list (e.g., genes with symbols starting with “mt”), since there were still several gene symbols that are common between human and mice, we decided to evaluate the potential association of all 134 genes with the infection process of coronavirus.

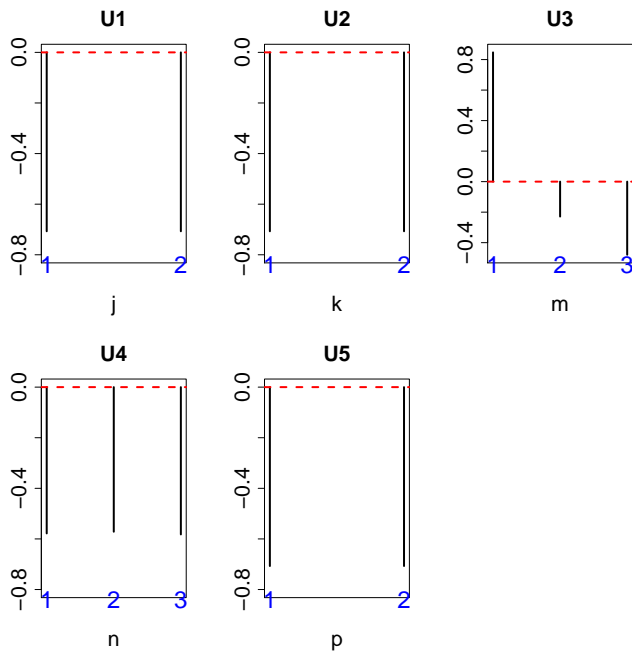


Fig. 3. Singular value vectors obtained by the HOSVD algorithm. U1: u_{1j} , U2: u_{1k} , U3: u_{2m} , U4: u_{1m} , and U5: u_{1p} . See Materials and Methods for the meanings of j, k, m, n , and p .

TABLE V
ONE HUNDRED AND THIRTY FOUR GENES SELECTED BY TD-BASED
UNSUPERVISED FE

Actb Actg1 Ahsg Alb Ambp Apoal Apoal2 Apoc1 Apoe B2m Bst2 C3
Cenblip1 Cd74 Cfb Eef1a1 Eef1g Eef2 Fabp1 Fau Fga Fgb Fgg Fth1 Ftl1
Gapdh Gc Gm10800 Gm2000 Gpx1 H2-Aa H2-D1 H2-K1 H2-T23 Hamp
Hba-a2 Hbb-bs Hbb-bt Hist1h3b Hist1h4h Hist2h2aa2 Hp Hpx Hsp90ab1
Hsp90b1 Hspa8 Ifi2712a Ifitm3 Lars2 Lcn2 Lyz2 mt-Atp6 mt-Atp8 mt-Co1
mt-Co2 mt-Co3 mt-Cytb mt-Nd1 mt-Nd2 mt-Nd3 mt-Nd4 Mt1 Mt2 Myh9
Orm1 Orm2 Pabpc1 Psap Ptma Rack1 Rpl10-ps3 Rpl11 Rpl12 Rpl13 Rpl13a
Rpl14 Rpl17 Rpl19 Rpl23a Rpl26 Rpl3 Rpl32 Rpl36 Rpl36a Rpl37a Rpl38
Rpl4 Rpl41 Rpl5 Rpl6 Rpl7 Rpl7a Rpl8 Rplp0 Rplp1 Rplp2 Rps11 Rps12
Rps14 Rps15 Rps17 Rps18 Rps2 Rps21 Rps23 Rps24 Rps27a Rps27rt Rps29
Rps3 Rps3a1 Rps4x Rps5 Rps6 Rps7 Rps8 Rps9 Rpsa S100a8 S100a9 Saa1
Saa2 Serpina1a Serpina1b Serpina1c Serpina1d Serpina3k Tmsb4x Tpt1 Trf
Ttr Ubb Ubc Wfdc21

C. Protein-protein interaction with coronavirus infection

We first evaluated whether the 134 selected genes could reflect the process of coronavirus infection using the Enrichr server for functional enrichment analysis. Several of the genes were enriched in the category “Virus-Host PPI P-HIPSTER 2020”, which is related to SARS-CoV (Table VI, see the supplementary materials for the full list).

These genes were also related to ORF1ab, polyprotein, and 3C-like protease. Interestingly, Woo et al. [5] suggested that ORF1ab, which encodes a replicase polyprotein of CoV-HKU1, is cleaved by papain-like proteases and 3C-like proteinase. Thus, it is reasonable that ORF1ab, polyprotein, and 3C-like protease would be affected during MHV infection VI. Other PPIs detected that are not listed in Table VI (see supplementary materials) were also mainly associated with ORF1ab and polyproteins, suggesting that our strategy has clear capability to elucidate the basic infectious process at the

molecular level that is common among various coronaviruses.

D. Virus perturbation

We next evaluated whether genes with known altered expression by virus perturbation overlapped with the 134 genes selected by our TD-based unsupervised FE approach (Table VII; see the supplementary material for the full list).

Among these, we detected the overlap of many genes that are perturbed in response to either SARS-CoV or SARS-like bat CoV, which are the genetically closest coronaviruses to the new SARS-CoV-2 strain. This further suggests that our results could have high similarity to the genes perturbed in SARS-CoV-2 infection.

E. TMPRSS2 as a scavenger receptor

For further functional enrichment analysis, we uploaded the 134 selected genes to Metascape to identify non-redundant biological terms (Fig. 4). Among the terms identified, “R-HSA-2173782: Binding and Uptake of Ligands by Scavenger Receptors” was the third most significantly enriched term. Although it was initially surprising that a scavenger receptor might be related to the response to coronavirus infection, a search of the related literature revealed that the scavenger receptor TMPRSS2 plays a critical role in SARS-CoV-2 infection as well as SARS-CoV infection [6]. Isolation of SARS-CoV-2 was also reported to be enhanced by TMPRSS2-expressing cells [7]. Moreover, TMPRSS2 contains a scavenger receptor domain [8], suggesting that TMPRSS2 activity would be related to detection of scavenger receptor activity. This finding further demonstrates the outstanding capability of our strategy to detect factors related to the SARS-CoV-2 infectious process. Moreover, this analysis suggests that research on the SARS-CoV infection process could be informative for understanding the SARS-CoV-2 infection process when it is not possible to directly investigate SARS-CoV-2 infection.

F. Drug discovery

We previously demonstrated that genes selected by TD-based unsupervised FE are useful to screen for drugs that are effective in treating disease or those that may cause adverse effects [9]. Therefore, we used this approach to screen for candidate drugs to treat coronavirus infections based on the individual terms that emerged from the Enrichr analysis.

1) *Drug Matrix*: In the Enrichr category “DrugMatrix”, the top-ranked drug was related to virus infection (Table VIII; see the supplementary materials for the full list). Most of these viruses are enveloped, single-stranded RNA viruses. Coronaviruses, including SARS-CoV-2, are positive-sense, enveloped, single-stranded RNA viruses, whereas influenza virus is a negative-sense, enveloped, single-stranded RNA virus.

Primaquine is known to inhibit the replication of Newcastle disease virus [10], which is in the family of paramyxoviruses that are enveloped, non-segmented, negative-sense single-stranded RNA viruses. Meloxicam is known to have cytotoxic and antiproliferative activity on virus-transformed tumor cells [11], including myelocytomatosis virus and Rous

TABLE VI
SARS-CoV-RELATED VIRUS PPI IN ENRICHR

Term	Overlap	P-value	Adjusted P-value
SARS coronavirus excised_polyprotein 1..4369 (gene: orf1ab)	10/194	7.52×10^{-7}	1.68×10^{-3}
SARS coronavirus P2_full_polyprotein 1..4382	10/198	9.06×10^{-7}	1.01×10^{-3}
SARS coronavirus nsp7-pp1a/pp1ab (gene: orf1ab)	4/36	9.61×10^{-5}	2.08×10^{-2}
SARS coronavirus 3C-like protease (gene: orf1ab)	3/19	2.63×10^{-4}	3.05×10^{-2}

TABLE VII
VIRUS PERTURBATION IN ENRICHER

Term	Overlap	P-value	Adjusted P-value
up			
SARS-ddORF6 24Hour GSE47961	10/300	3.52×10^{-5}	3.79×10^{-3}
cSARS Bat SRBD 60Hour GSE37827	9/300	1.93×10^{-4}	1.04×10^{-2}
SARS-BatSRBD 60Hour GSE47961	8/300	9.51×10^{-4}	4.38×10^{-2}
down			
SARS-BatSRBD 96Hour GSE47960	11/300	5.77×10^{-6}	4.66×10^{-4}
SARS-BatSRBD 84Hour GSE47960	9/300	1.93×10^{-4}	6.24×10^{-3}
cSARS Bat SRBD 60Hour GSE37827	8/300	9.51×10^{-4}	2.36×10^{-2}

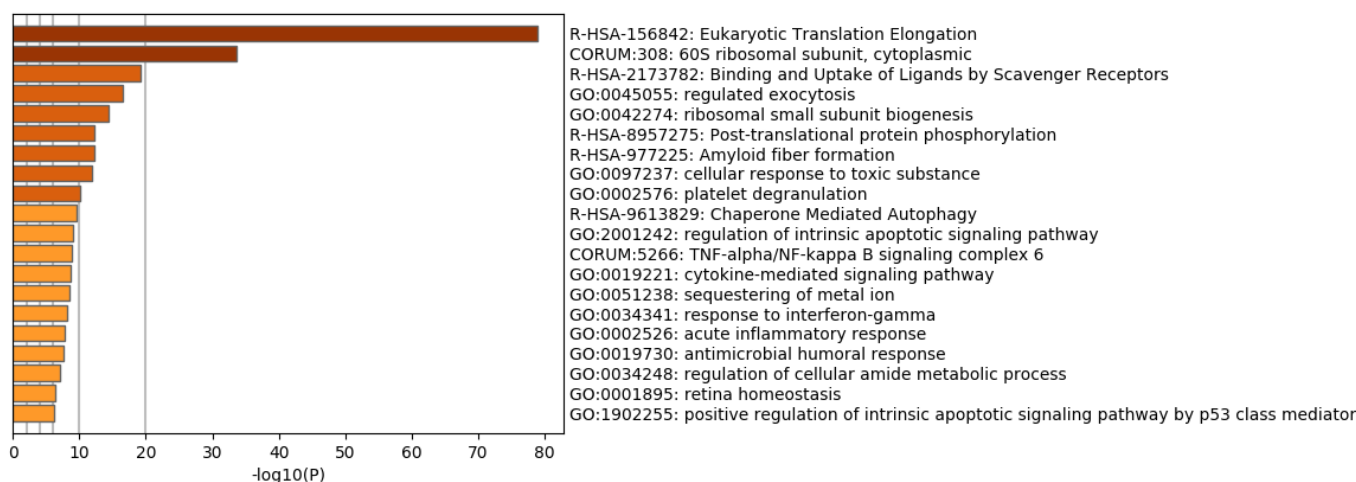


Fig. 4. Redundant heatmap of enriched terms generated by uploading the selected 134 genes to Metascape

TABLE VIII
DRUGS ENRICHR IN THE “DRUGMATRIX” CATEGORY IN ENRICHR. THE FULL LIST IS AVAILABLE IN THE SUPPLEMENTARY MATERIAL

Term	Overlap	P-value	Adjusted P-value
Primaquine-45 mg/kg in CMC-Rat-Liver-5d-up	23/315	1.40×10^{-17}	1.10×10^{-13}
Meloxicam-33 mg/kg in Corn Oil-Rat-Kidney-1d-up	23/337	6.19×10^{-17}	2.44×10^{-13}
Cytarabine-487 mg/kg in Saline-Rat-Liver-0.25d-up	22/300	6.87×10^{-17}	1.80×10^{-13}
Clotrimazole-60 uM in DMSO-Rat-Primary rat hepatocytes-0.67d-dn	24/381	7.59×10^{-17}	1.49×10^{-13}
Diclofenac-3.5 mg/kg in Corn Oil-Rat-Liver-5d-dn	21/269	1.04×10^{-16}	1.64×10^{-13}
Pyrogallol-1000 mg/kg in Water-Rat-Liver-3d-up	23/349	1.33×10^{-16}	1.75×10^{-13}
Clindamycin-161 mg/kg in Saline-Rat-Kidney-1d-up	23/366	3.76×10^{-16}	4.23×10^{-13}
Catechol-195 mg/kg in Saline-Rat-Liver-0.25d-up	21/290	4.76×10^{-16}	4.69×10^{-13}
Anisindione-75 mg/kg in CMC-Rat-Liver-5d-up	21/295	6.72×10^{-16}	5.88×10^{-13}
Phenylhydrazine-78 mg/kg in Water-Rat-Liver-3d-up	22/335	7.00×10^{-16}	5.51×10^{-13}
N-Nitrosodiethylamine-1.67 mg/kg in Saline-Rat-Liver-0.25d-up	23/377	7.15×10^{-16}	5.12×10^{-13}
Neomycin-56 mg/kg in Corn Oil-Rat-Liver-1d-dn	20/259	7.28×10^{-16}	4.78×10^{-13}

sarcoma virus. Myelocytomatosis virus is a retrovirus, which is an enveloped, negative-sense, single-stranded RNA virus, whereas Rous sarcoma virus is an enveloped, positive-sense, single-stranded RNA virus. Although there are no studies showing that cytarabine is effective against infection of an RNA virus, one report demonstrated that cytarabine can affect DNA virus infection [12]. Pyrogallol was reported to have

anti-virus effects on human influenza virus strain A/Udorn/72, avian influenza virus A/swan/Shimane/499/83, herpes simplex virus-1, vesicular stomatitis virus, and retrovirus [13]. As mentioned above, influenza virus is a negative-sense, enveloped, single-stranded RNA virus; herpesvirus is a DNA virus; vesicular stomatitis virus is an enveloped, single-stranded, negative-sense RNA virus; and retroviruses are enveloped,

negative-sense, single-stranded RNA viruses. This suggests that a single drug can effectively inhibit a wide range of viruses from DNA viruses to both negative- and positive-sense RNA viruses. The structure-dependent antiviral activity of catechol derivatives in pyroligneous acid against encephalomyocarditis virus was reported, which is a non-enveloped single-stranded RNA virus [14]. To our knowledge, there are no reports that neomycin is effective against RNA viruses; however, one study showed that it could inhibit infection of fibroblasts with human cytomegalovirus [15], which is a DNA virus.

Although not all viruses identified to be related to the 134 genes selected by TD-based unsupervised FE are enveloped, positive-sense, single-stranded RNA viruses similar to SARS-CoV-2, since drugs shown to be effective against other viruses (e.g., DNA viruses) are also often effective against RNA viruses (including pyrogallol that was screened by our strategy), drugs in Table VIII warrant being tested as potential treatments for SARS-CoV-2 infection.

2) *Drug Perturbations from GEO*: Several promising drug compound candidates were also screened from the GEO “Drug Perturbations from GEO up” and “Drug Perturbations from GEO down” categories, along with available evidence for possible adverse effects (Table IX; see the supplementary material for the full list).

Drugs associated with upregulated genes that overlapped with the 134 genes selected by TD-based unsupervised FE are considered to be more likely to cause adverse effects, since they will enhance the expression of genes altered by SARS-CoV infection. Captopril is an angiotensin-converting enzyme (ACE) inhibitor, which is known to activate ACE2 that is the receptor that SARS-CoV-2 uses to infect human cells [16], suggesting that this drug might have negative effects for COVID-19 therapy. Coenzyme Q10, which frequently emerged in Table IX, has been reported to accelerate virus infection [17], which could therefore also have negative effects for COVID-19 therapy. Fenretinide is known to effectively inhibit HIV infection [18], and therefore might be a promising drug candidate for SARS-CoV-2 even though it was listed in the “Drug Perturbations from GEO up” category.

In contrast to the drugs in the above list, those associated with downregulated genes that overlapped with the 134 genes selected by TD-based unsupervised FE are considered to be able to effectively suppress SARS-CoV-2 infection, since they will inhibit the expression of genes altered by SARS-CoV infection. Pioglitazone was also included in the list of candidate compounds for SARS-CoV-2 screened by an *in silico* method [19]. Quercetin was reported to inhibit the cell entry of SARS-CoV-2 [20], and was also included in the list of candidate compounds for SARS-CoV-2 screened by an *in silico* method [21]. Fenretinide was also included in the drugs identified as effective compounds in the “Drug perturbations from GEO up” category as described above. Decitabine is one of the drugs used in HIV combination therapy [22]. Troglitazone impedes the oligomerization of sodium taurocholate co-transporting polypeptide and entry of hepatitis B virus into hepatocytes [23], which is a partially double-stranded DNA virus. Finally, motexafin gadolinium was reported to selectively induce apoptosis in HIV-1-infected

CD4+ T helper cells [24].

Based on these observations, our strategy appears to be useful to identify potential drug compounds for SARS-CoV-2.

G. Comparison with *in silico* drug discovery

Finally, we compared the drugs screened out using our approach from the “Drug perturbations from GEO up/down” lists with those screened from two *in silico* drug discovery studies [19], [21]

1) *Comparison with Wu et al. [19]*: We found multiple hits, which are summarized in Table X. The main drugs identified included doxycycline, ascorbic acid, isotretinoin, pioglitazone, cortisone, and tibolone.

Wu et al. [19] identified 29 potential PLpro inhibitors, 27 potential 3CLpro inhibitors, and 20 potential RdRp inhibitors from the ZINC drug database, and identified 13 potential PLpro inhibitors, 26 potential 3CLpro inhibitors, and 20 potential RdRp inhibitors from their in-house natural product database. Doxycycline was among both the potential PLpro and 3CLpro inhibitors; ascorbic acid and isotretinoin were among the potential PLpro inhibitors; pioglitazone was among the potential 3CLpro inhibitors; and cortisone and tibolone were included in the potential RdRp inhibitors from the ZINC drug database. These multiple hits also further support the suitability of our strategy.

2) *Comparison with Ubani et al. [21]*: Ubani et al. [21] screened a library of 22 phytochemicals with antiviral activity obtained from the PubChem database for activity against the spike envelope glycoprotein and main protease of SARS-CoV-2. Among these, we found only one hit that overlapped with our screened out drugs, which was quercetin (Table XI).

IV. DISCUSSION AND CONCLUSION

In this paper, we present a novel evaluation method to identify drugs that could be used to effectively treat COVID-19. We applied a TD-based unsupervised FE method to select genes with altered expression caused by MHV infection in mice. Although the dataset analyzed for this study was not based on SARS-CoV-2 infection, the 134 genes selected by TD-based unsupervised FE can still be considered useful for gaining a better understanding of the infectious mechanism of SARS-CoV-2 for several reasons. First, the 134 genes selected were enriched in general RNA virus proteins that play important roles during infectious processes. This suggests that the infectious mechanism represented by the 134 genes in the mouse model is also applicable to SARS-CoV-2 infection. In fact, these genes were also enriched in processes related to scavenger receptor activity, which might reflect the critical role of TMPRSS2 activity in SARS-CoV-2 replication, suggesting a potential therapeutic target.

Following these achievements, we tried to identify potential drug candidate compounds that could influence the 134 selected genes. Among these, we screened out several candidate compounds that are known antiviral drugs, including those that were screened out as drug candidate compounds for SARS-CoV-2 using *in silico* methods.

TABLE IX

DRUGS IDENTIFIED IN “DRUG PERTURBATIONS FROM GEO UP/DOWN” IN ENRICHR FOR THE 134 GENES SELECTED BY TD-BASED UNSUPERVISED FE.

Term	Overlap	P-value	Adjusted P-value
Drug Perturbations from GEO up			
coenzyme Q10 5281915 mouse GSE15129 sample 3464	64/302	1.32×10^{-81}	1.20×10^{-78}
coenzyme Q10 5281915 mouse GSE15129 sample 3456	63/396	1.05×10^{-71}	4.78×10^{-69}
captopril DB01197 mouse GSE19286 sample 2689	47/134	1.76×10^{-70}	5.33×10^{-68}
ubiquinol 9962735 mouse GSE15129 sample 3463	60/346	2.28×10^{-70}	5.15×10^{-68}
N-METHYLFORMAMIDE 31254 rat GSE5509 sample 3570	56/283	8.87×10^{-69}	1.61×10^{-66}
1-Naphthyl isothiocyanate 11080 rat GSE5509 sample 3568	56/301	3.80×10^{-67}	5.73×10^{-65}
fenretinide 5288209 rat GSE3952 sample 3561	59/397	6.98×10^{-65}	9.04×10^{-63}
coenzyme Q10 5281915 mouse GSE15129 sample 3462	50/257	1.49×10^{-60}	1.69×10^{-58}
bexarotene DB00307 human GSE6914 sample 2680	43/147	3.03×10^{-60}	3.05×10^{-58}
FENRETINIDE 5288209 rat GSE3952 sample 3563	52/345	5.99×10^{-57}	5.42×10^{-55}
Drug Perturbations from GEO up			
pioglitazone DB01132 rat GSE21329 sample 2841	56/321	1.85×10^{-65}	1.67×10^{-62}
quercetin DB04216 mouse GSE38067 sample 3441	59/486	1.81×10^{-59}	8.19×10^{-57}
ubiquinol 9962735 mouse GSE15129 sample 3461	53/349	2.64×10^{-58}	7.95×10^{-56}
fenretinide 5288209 rat GSE3952 sample 3559	56/440	2.31×10^{-57}	5.21×10^{-55}
decitabine 451668 mouse GSE4768 sample 3108	45/226	1.06×10^{-54}	1.91×10^{-52}
troglitazone DB00197 rat GSE21329 sample 2832	50/355	4.51×10^{-53}	6.79×10^{-51}
adenosine triphosphate 5957 human GSE30903 sample 3219	49/341	2.16×10^{-52}	2.78×10^{-50}
alitreinoin DB00523 rat GSE3952 sample 2673	53/483	1.54×10^{-50}	1.74×10^{-48}
bexarotene 82146 rat GSE3952 sample 3560	48/361	1.42×10^{-49}	1.43×10^{-47}
HYPOCHLOROUS ACID 24341 human GSE11630 sample 3201	41/221	2.67×10^{-48}	2.41×10^{-46}
streptozocin DB00428 mouse GSE38067 sample 3439	44/287	4.40×10^{-48}	3.61×10^{-46}
rosiglitazone DB00412 mouse GSE35011 sample 2813	44/290	7.13×10^{-48}	5.36×10^{-46}
motexafin gadolinium (4 h) DB05428 human GSE2189 sample 3125	43/302	1.70×10^{-45}	1.18×10^{-43}

TABLE X

LIST OF *in silico* SCREENED DRUGS [19] WHOSE TARGET GENES WERE ALSO ENRICHED IN THE 134 GENES SELECTED BY TD-BASED UNSUPERVISED FE.

Term	Overlap	P-value	Adjusted P-value
Drug Perturbations from GEO up			
doxycycline DB00254 mouse GSE29848 sample 3209	32/267	3.73×10^{-31}	3.56×10^{-30}
doxycycline DB00254 human GSE2624 sample 3074	28/175	6.59×10^{-31}	6.22×10^{-30}
doxycycline DB00254 human GSE2624 sample 3077	27/209	3.34×10^{-27}	2.46×10^{-26}
doxycycline DB00254 human GSE2624 sample 3076	25/272	1.71×10^{-21}	8.32×10^{-21}
doxycycline DB00254 mouse GSE29848 sample 3207	22/225	1.40×10^{-19}	6.10×10^{-19}
doxycycline DB00254 mouse GSE29848 sample 3208	12/291	6.24×10^{-7}	1.40×10^{-6}
ascorbic acid 54670067 human GSE11919 sample 3190	8/313	1.25×10^{-3}	2.33×10^{-3}
isotretinoin DB00982 human GSE10432 sample 2772	8/308	1.13×10^{-3}	2.11×10^{-3}
pioglitazone DB01132 rat GSE21329 sample 2843	48/400	2.31×10^{-47}	7.49×10^{-46}
pioglitazone DB01132 rat GSE21329 sample 2842	42/349	3.21×10^{-41}	6.19×10^{-40}
pioglitazone DB01132 rat GSE21329 sample 2842	42/349	3.21×10^{-41}	6.19×10^{-40}
pioglitazone DB01132 rat GSE20219 sample 2794	13/292	8.57×10^{-8}	2.01×10^{-7}
pioglitazone 4829 mouse GSE1458 sample 2587	11/318	1.00×10^{-5}	2.13×10^{-5}
pioglitazone DB01132 mouse GSE32536 sample 2797	7/307	4.69×10^{-3}	8.40×10^{-3}
pioglitazone DB01132 rat GSE20219 sample 2795	7/330	6.90×10^{-3}	1.22×10^{-2}
hydrocortisone DB00741 human GSE7890 sample 2751	40/305	1.01×10^{-40}	1.75×10^{-39}
tibolone 444008 human GSE12446 sample 3204	15/287	9.26×10^{-10}	2.38×10^{-9}
Drug Perturbations from GEO down			
doxycycline DB00254 human GSE2624 sample 3075	20/358	3.39×10^{-13}	1.34×10^{-12}
doxycycline DB00254 mouse GSE29848 sample 3208	17/309	2.91×10^{-11}	1.02×10^{-10}
doxycycline DB00254 human GSE2624 sample 3077	18/391	1.37×10^{-10}	4.58×10^{-10}
doxycycline DB00254 mouse GSE29848 sample 3207	17/375	5.85×10^{-10}	1.86×10^{-9}
doxycycline DB00254 human GSE2624 sample 3074	17/425	3.88×10^{-9}	1.16×10^{-8}
doxycycline DB00254 mouse GSE29848 sample 3209	9/333	4.16×10^{-4}	8.91×10^{-4}
ascorbic acid 54670067 human GSE11919 sample 3190	19/287	6.71×10^{-14}	2.75×10^{-13}
Ascorbic acid 54670067 mouse GSE37676 sample 3132	15/306	2.23×10^{-9}	6.89×10^{-9}
pioglitazone DB01132 rat GSE21329 sample 2841	56/321	1.85×10^{-65}	1.67×10^{-62}
pioglitazone 4829 mouse GSE1458 sample 2587	28/282	5.89×10^{-25}	5.26×10^{-24}
pioglitazone DB01132 rat GSE20219 sample 2794	25/308	3.62×10^{-20}	2.25×10^{-19}
pioglitazone DB01132 rat GSE20219 sample 2795	21/270	1.12×10^{-16}	5.41×10^{-16}
pioglitazone DB01132 human GSE8157 sample 2796	12/269	2.70×10^{-7}	7.17×10^{-7}
tibolone 444008 human GSE12446 sample 3204	35/313	4.90×10^{-33}	8.68×10^{-32}

One might wonder if MHV is a suitable model to be consider SARS-CoV-2 infection, since there are more data set

available for SARS-CoV infection toward mouse lung. In order to evaluate the suitability of MHV as model of SARS-CoV-

TABLE XI

LIST OF *in silico* SCREENED DRUGS [21] WHOSE TARGET GENES ARE ALSO ENRICHED IN THE 134 GENES SELECTED BY TD BASED UNSUPERVISED FE.

Term	Overlap	P-value	Adjusted P-value
Drug Perturbations from GEO up			
quercetin DB04216 mouse GSE38141 sample 3435	33/280	6.85×10^{-32}	6.74×10^{-31}
quercetin DB04216 mouse GSE38136 sample 3438	31/254	1.99×10^{-30}	1.80×10^{-29}
quercetin DB04216 mouse GSE38136 sample 3437	37/472	2.85×10^{-29}	2.37×10^{-28}
quercetin 5280343 rat GSE7479 sample 3409	33/394	5.47×10^{-27}	3.97×10^{-26}
quercetin DB04216 mouse GSE38136 sample 3436	30/297	5.97×10^{-27}	4.29×10^{-26}
quercetin DB04216 mouse GSE38067 sample 3440	26/227	8.02×10^{-25}	4.88×10^{-24}
quercetin 5280343 human GSE7259 sample 3416	29/327	1.99×10^{-24}	1.17×10^{-23}
quercetin DB04216 mouse GSE38067 sample 3441	20/114	4.34×10^{-23}	2.37×10^{-22}
quercetin 5280343 human GSE13899 sample 3182	16/307	2.56×10^{-10}	6.85×10^{-10}
quercetin DB04216 mouse GSE4262 sample 3428	14/360	1.42×10^{-7}	3.29×10^{-7}
quercetin DB04216 mouse GSE4262 sample 3429	9/229	2.44×10^{-5}	5.14×10^{-5}
quercetin 5280343 human GSE7259 sample 3415	9/336	4.44×10^{-4}	8.58×10^{-4}
quercetin DB04216 mouse GSE4262 sample 3433	8/323	1.52×10^{-3}	2.82×10^{-3}
quercetin DB04216 mouse GSE4262 sample 3434	8/324	1.55×10^{-3}	2.87×10^{-3}
quercetin DB04216 mouse GSE4262 sample 3431	7/252	1.56×10^{-3}	2.89×10^{-3}
quercetin DB04216 mouse GSE4262 sample 3427	8/360	2.97×10^{-3}	5.40×10^{-3}
quercetin DB04216 mouse GSE4262 sample 3432	5/254	2.83×10^{-3}	4.76×10^{-3}
Drug Perturbations from GEO down			
quercetin DB04216 mouse GSE38067 sample 3441	59/486	1.81×10^{-59}	8.19×10^{-57}
quercetin DB04216 mouse GSE38136 sample 3437	26/128	1.33×10^{-31}	2.00×10^{-30}
quercetin 5280343 human GSE7259 sample 3415	29/264	4.05×10^{-27}	4.57×10^{-26}
quercetin DB04216 mouse GSE38136 sample 3436	30/303	1.09×10^{-26}	1.17×10^{-25}
quercetin 5280343 human GSE13899 sample 3182	26/293	6.10×10^{-22}	4.55×10^{-21}
quercetin DB04216 mouse GSE38067 sample 3440	28/373	1.31×10^{-21}	9.44×10^{-21}
quercetin DB04216 mouse GSE38136 sample 3438	27/346	2.71×10^{-21}	1.91×10^{-20}
quercetin DB04216 mouse GSE38141 sample 3435	22/320	2.68×10^{-16}	1.26×10^{-15}
quercetin 5280343 human GSE7259 sample 3416	18/273	3.44×10^{-13}	1.36×10^{-12}
quercetin 5280343 rat GSE7479 sample 3409	14/206	1.12×10^{-10}	3.81×10^{-10}
quercetin DB04216 mouse GSE4262 sample 3431	11/348	2.31×10^{-5}	5.47×10^{-5}
quercetin DB04216 mouse GSE4262 sample 3427	5/240	2.28×10^{-3}	4.21×10^{-3}

2 infectious process, we also performed additional analyses using two SARS-CoV infectious processes toward mouse lung (see Materials and Methods). As can be seen in Figs. 5 and 6, $\ell_1 = 2$ is selected as singular value vector $u_{\ell_1 j}$ that has monotonic dependence upon j , $\ell_2 = 2$ is selected as singular value vector $u_{\ell_2 k}$ that has monotonic dependence upon k , and $\ell_3 = 1$ is selected as singular value vector $u_{\ell_3 n}$ that has constant values regardless n for GSE33266 while $\ell_1 = 2$ is selected as singular value vector $u_{\ell_1 j}$ that has distinct values between Mock ($j = 3$) and infectious samples ($j = 1, 2$), $\ell_2 = 3$ is selected as singular value vector $u_{\ell_2 k}$ that has monotonic dependence upon k , and $\ell_3 = 1$ is selected as singular value vector $u_{\ell_3 n}$ that has constant values regardless n for GSE50000. Then $\ell_4 = 2, 3$ and $\ell_4 = 1$ are selected as those associated with the larger absolute values of $G(\ell_1 \ell_2 \ell_3 \ell_4)$ given ℓ_1, ℓ_2, ℓ_3 . P -values, P_i , are attributed to gene i using cumulative χ^2 distribution, $P_{\chi^2}[> x]$, as described in Materials and Methods, 569 and 475 gene symbols associated with selected genes are selected for GSE33266 and GSE50000, respectively (see supplementary materials). Figure 7 shows Venn diagram of these two sets of genes and 134 genes selected by TD based unsupervised FE using GSE146074. Although there are some overlaps, majority of genes are not shared among these three gene sets.

These two sets of genes are uploaded to Enrichr and it is checked if they are significantly overlapped with corona virus PPI genes (Table XII). It is obvious that two sets of selected genes are significantly overlapping with genes that are

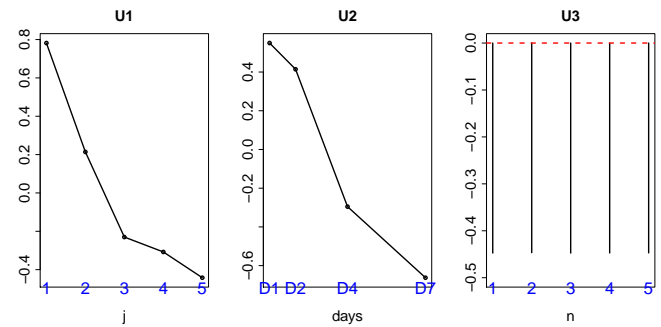


Fig. 5. Singular value vectors obtained by the HOSVD algorithm applied to GSE33266 (Table II). U1: $u_{\ell_1 j}$, U2: $u_{\ell_2 k}$, and U3: $u_{\ell_3 n}$. See Materials and Methods for the meanings of j, k and n .

supposed to interact with SARS-CoV proteins in spite of that these two gene sets are not highly coincident with 134 genes selected by TD based unsupervised FE using GSE146074 (Fig. 7). This means that TD based unsupervised FE generally has ability to predict PPI using gene expression profiles no matter which data sets are used. It also suggests that the achievement in Table VI is not unlikely accidental but really an evidence that genes selected by TD based unsupervised FE are those interacting with SARS-CoV proteins during infectious processes.

A possible another concern is that the studies are not based upon direct investigation of SARS-CoV-2 but based upon on that of closely related virus. This suggests that everything

TABLE XII
SARS-CoV-RELATED VIRUS PPI IN ENRICHR

Term	Overlap	P-value	Adjusted P-value
GSE33266			
SARS coronavirus excised_polyprotein 1.4369 (gene: orf1ab)	16/194	3.21×10^{-6}	1.54×10^{-3}
SARS coronavirus P2 full_polyprotein 1.4382	16/198	4.18×10^{-6}	1.65×10^{-3}
SARS coronavirus nsp9-pp1a/pp1ab (gene: orf1ab)	5/13	4.26×10^{-6}	1.59×10^{-3}
SARS coronavirus 3C-like proteinase (gene: orf1ab)	5/19	3.47×10^{-5}	4.09×10^{-3}
SARS coronavirus nsp8-pp1a/pp1ab (gene: orf1ab)	7/45	3.67×10^{-5}	4.18×10^{-3}
SARS coronavirus 2-O-ribose methyltransferase (2-o-MT) (gene: orf1ab)	4/11	5.42×10^{-5}	4.73×10^{-3}
SARS coronavirus nsp7-pp1a/pp1ab (gene: orf1ab)	6/36	8.97×10^{-5}	6.77×10^{-3}
SARS coronavirus endoRNase (gene: orf1ab)	3/6	1.71×10^{-4}	1.11×10^{-2}
SARS coronavirus nsp4-pp1a/pp1ab (gene: orf1ab)	4/16	2.75×10^{-4}	1.61×10^{-2}
SARS coronavirus formerly known as growth-factor-like protein (gene: orf1ab)	4/17	3.54×10^{-4}	1.93×10^{-2}
SARS coronavirus Tor2 replicase 1AB	9/108	4.26×10^{-4}	2.22×10^{-2}
SARS coronavirus P2 full_polyprotein 1.7073	9/109	4.56×10^{-4}	2.32×10^{-2}
SARS coronavirus RNA-dependent RNA polymerase (gene: orf1ab)	3/9	6.84×10^{-4}	2.94×10^{-2}
SARS coronavirus leader protein (gene: orf1ab)	4/20	6.86×10^{-4}	2.92×10^{-2}
SARS coronavirus nsp3-pp1a/pp1ab (gene: orf1ab)	9/118	8.12×10^{-4}	3.22×10^{-2}
GSE50000			
SARS coronavirus 3C-like proteinase (gene: orf1ab)	4/19	4.21×10^{-4}	1.62×10^{-2}
SARS coronavirus hypothetical protein sars7a	5/38	7.75×10^{-4}	1.94×10^{-2}
SARS coronavirus P2 hypothetical protein sars7a	5/38	7.75×10^{-4}	1.94×10^{-2}
SARS coronavirus Tor2 Orf8	5/38	7.75×10^{-4}	1.93×10^{-2}
SARS coronavirus 2-O-ribose methyltransferase (2-o-MT) (gene: orf1ab)	3/11	1.05×10^{-3}	2.12×10^{-2}
SARS coronavirus nsp9-pp1a/pp1ab (gene: orf1ab)	3/13	1.77×10^{-3}	2.43×10^{-2}
SARS coronavirus nsp13-pp1ab (ZD, NTPase/HEL; RNA (gene: orf1ab)	3/14	2.22×10^{-3}	2.49×10^{-2}
SARS coronavirus P2 spike glycoprotein precursor	6/71	2.48×10^{-3}	2.69×10^{-2}
SARS coronavirus E2 glycoprotein precursor (gene: S)	6/72	2.66×10^{-3}	2.78×10^{-2}
SARS coronavirus Tor2 spike glycoprotein	6/72	2.66×10^{-3}	2.78×10^{-2}
SARS coronavirus nsp4-pp1a/pp1ab (gene: orf1ab)	3/16	3.31×10^{-3}	2.94×10^{-2}
SARS coronavirus nsp3-pp1a/pp1ab (gene: orf1ab)	7/118	7.99×10^{-3}	3.74×10^{-2}

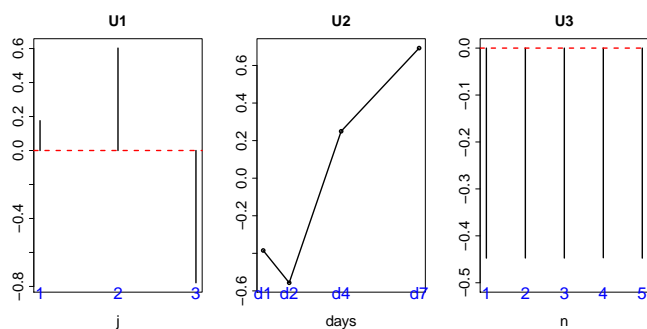


Fig. 6. Singular value vectors obtained by the HOSVD algorithm applied to GSE50000 (Table II). U1: u_{2j} , U2: u_{3k} , and U3: u_{1n} . See Materials and Methods for the meanings of j , k and n .

identified here might not be applicable to SARS-CoV-2 at all. In order to address this point, we compare the 134 genes (Table V) with genes reported to be interacting with SARS-CoV-2 proteins [25] (Table XIII). It is obvious that 134 genes are significantly overlapping with human genes reported to be interacting with SARS-CoV-2 proteins. This means that TD based unsupervised FE has ability to predict PPI even when only gene expression profiles during related virus infection are available.

Finally, we also compared identified drugs (“Drug Pert GEO up/down” and “DrugMarix” in supplementary materials) with those reported to be possible drugs toward SARS-CoV-2 [26]. Among 142 drugs identified by Zhou et al [26], as many as 25 drugs were found to significantly affect 134 genes in at

TABLE XIII
COINCIDENCE BETWEEN 134 GENES AND HUMAN GENES REPORTED TO BE INTERACTING WITH SARS-CoV-2 PROTEINS [25]

SARS-CoV-2 proteins	P values	Odds Ratio
SARS-CoV2 E	1.59×10^{-41}	20.2
SARS-CoV2 M	1.53×10^{-34}	13.7
SARS-CoV2 N	1.69×10^{-51}	31.8
SARS-CoV2 nsp1	5.56×10^{-33}	19.8
SARS-CoV2 nsp10	4.16×10^{-32}	23.0
SARS-CoV2 nsp11	3.59×10^{-41}	19.1
SARS-CoV2 nsp12	4.29×10^{-31}	18.3
SARS-CoV2 nsp13	7.26×10^{-42}	18.6
SARS-CoV2 nsp14	1.64×10^{-32}	22.3
SARS-CoV2 nsp15	3.72×10^{-26}	16.4
SARS-CoV2 nsp2	5.25×10^{-48}	22.7
SARS-CoV2 nsp4	2.18×10^{-35}	16.0
SARS-CoV2 nsp5	4.30×10^{-40}	25.5
SARS-CoV2 nsp5_C145A	8.22×10^{-31}	25.1
SARS-CoV2 nsp6	1.52×10^{-36}	16.0
SARS-CoV2 nsp7	6.93×10^{-31}	14.7
SARS-CoV2 nsp8	3.51×10^{-44}	19.6
SARS-CoV2 nsp9	2.62×10^{-42}	23.3
SARS-CoV2 orf10	2.67×10^{-46}	22.3
SARS-CoV2 orf3a	8.57×10^{-44}	19.8
SARS-CoV2 orf3b	3.79×10^{-47}	24.8
SARS-CoV2 orf6	1.51×10^{-42}	21.9
SARS-CoV2 orf7a	6.28×10^{-34}	15.3
SARS-CoV2 orf8	1.90×10^{-33}	14.0
SARS-CoV2 orf9b	3.16×10^{-42}	22.3
SARS-CoV2 orf9c	8.73×10^{-38}	13.9
SARS-CoV2 Spike	5.35×10^{-36}	17.8

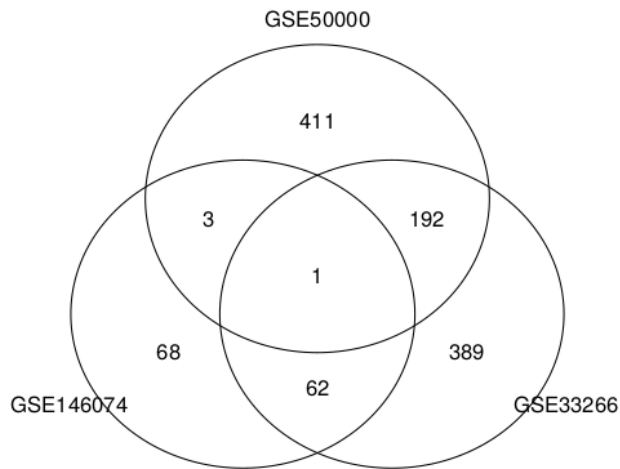


Fig. 7. Venn diagrams of 134 genes selected by TD bases unsupervised FE using GSE146074, 569 genes selected by TD bases unsupervised FE using GSE33266, and 475 genes selected by TD bases unsupervised FE using GSE50000.

TABLE XIV

NUMBER OF EXPERIMENTS ASSOCIATED WITH ADJUSTED P -VALUES IN VARIOUS ENRICHR CATEGORIES FOR THE DRUGS IDENTIFIED IN ANOTHER STUDY[26]

	GEO up	GEO down	DrugMatrix
Methotrexate	2	1	35
Fluorouracil	4	5	3
Testosterone	1		12
Stanolone	2	1	
Menadione		1	
Hydrocortisone		1	20
Mestranol			6
Hexestrol			4
Mercaptopurine			15
Paroxetine			8
Vinblastine			16
Phenylbutazone			3
Naloxone			6
Hydralazine			11
Vinorelbine			10
Carvedilol			16
Colchicine			12
Amitriptyline			12
Epinephrine			12
Dactinomycin			6
Melatonin			8
Methyltestosterone			6
Omeprazole			19
Oxymetholone			6
Progesterone			20

least one experiment within either DrugMatrix, or GEO, in Enrichr with adjusted P -values less than 0.05 (XIV). Thus, our proposal of drug repositioning is also reliable.

Since it is unlikely that this level of agreements mentioned in the above is purely accidental, the drugs identified in the present study can be useful candidates for further evaluation in COVID-19 therapy. This work therefore provides a foundation for further research pertaining to utilizing advanced learning concepts to analyze COVID-19 infectious disease.

Final concerns to be addressed might be the comparison

with other methods applied to synthetic data sets than TD based unsupervised FE. When considering synthetic data set, categorical regression, eq. (10), outperformed TD based unsupervised FE. Although eq. (9) cannot be better than TD based unsupervised FE (Table III), it is still comparative. If these two more easily understood methods are better than or comparative to TD based unsupervised FE, TD based unsupervised FE, which is more difficult to interpret, is useless. In order to check this point, we applied categorical regression and eq. (9), which are modified as

$$x_{ijk mnp} = \sum_{j'=1}^2 \sum_{k'=1}^2 \sum_{m'=1}^3 \alpha_{ij'k'm'} \delta_{jj'} \delta_{kk'} \delta_{mm'} + \gamma_i'' \quad (13)$$

and

$$x_{ijk mnp} = \alpha'_i a_j b_k c_m + \gamma'_i \quad (14)$$

where $a_i = i, b_k = k, c_m = m$, to the present set (GSE146074). Then i s associated with adjusted P -values less than 0.01 are selected; it turned out that there are too many genes that pass this screening, 25609 and 20217, respectively. This suggests that these two methods lack the ability to screen limited number of genes that are likely interacting SARS-CoV-2 proteins, since not most of genes but only limited number of human genes are interacting SARS-CoV-2 proteins (2×10^4 are as many as all of human protein coding genes). Although this fact is enough to deny to employ these two methods replaced with TD based unsupervised FE, we still seek other possibility; even if these two methods fail to screen limited number of genes, if only top ranked genes are selected, it might be possible to select limited number of genes that significantly overlap with genes reported to interact with SARS-CoV-2 proteins. In order to see this, we select top ranked 134 gene using P -values that these two methods compute and upload them to Enrichr. Nevertheless, we found that there are no SARS-CoV-2 proteins that significantly interact with these uploaded 134 genes. Since the significant interaction with SARS-CoV-2 proteins is the primary requirement for genes to be used to screen candidate drug compounds, these two methods are definitely useless for the present purpose.

If we employ more complicated and sophisticated methods to select genes, it might be possible for us to have limited number of genes that significantly interact with SARS-CoV-2 protein. Nonetheless, since TD based unsupervised FE is simple and rapid (see cpu time in Table III) enough to achieve the present purpose, we are not willing to test more complicated and advanced methods in the present study.

ACKNOWLEDGMENT

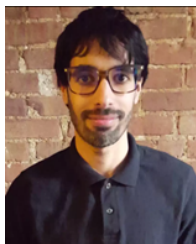
This study was supported by KAKENHI grants 19H05270, 20H04848, and 20K12067. This project was also funded by the Deanship of Scientific Research (DSR) at King Abdulaziz University, Jeddah, under grant no. KEP-8-611-38. The authors, therefore, acknowledge DSR with thanks for providing technical and financial support.

REFERENCES

- [1] S. Pfaender, K. B. Mar, E. Michailidis, A. Kratzel, D. Hirt, P. V'kovski, W. Fan, N. Ebert, H. Stalder, H. Kleine-Weber, M. Hoffmann, H. H. Hoffmann, M. Saeed, R. Dijkman, E. Steinmann, M. Wight-Carter, N. W. Hanners, S. Pöhlmann, T. Gallagher, D. Todt, G. Zimmer, C. M. Rice, J. W. Schoggins, and V. Thiel, "LY6E impairs coronavirus fusion and confers immune control of viral disease," *bioRxiv*, 2020. [Online]. Available: <https://www.biorxiv.org/content/early/2020/03/07/2020.03.05.979260>
- [2] Y. h. Taguchi, *Unsupervised feature extraction applied to bioinformatics: PCA and TD based approach*. Switzerland: Springer International, 2020.
- [3] M. V. Kuleshov, M. R. Jones, A. D. Rouillard, N. F. Fernandez, Q. Duan, Z. Wang, S. Koplev, S. L. Jenkins, K. M. Jagodnik, A. Lachmann, M. G. McDermott, C. D. Monteiro, G. W. Gundersen, and A. Ma'ayan, "Enrichr: a comprehensive gene set enrichment analysis web server 2016 update," *Nucleic Acids Research*, vol. 44, no. W1, pp. W90–W97, 05 2016. [Online]. Available: <https://doi.org/10.1093/nar/gkw377>
- [4] Y. Zhou, B. Zhou, L. Pache, M. Chang, A. H. Khodabakhshi, O. Tanaseichuk, C. Benner, and S. K. Chanda, "Metascape provides a biologist-oriented resource for the analysis of systems-level datasets," *Nature Communications*, vol. 10, no. 1, apr 2019. [Online]. Available: <https://doi.org/10.1038/s41467-019-09234-6>
- [5] P. C. Woo, Y. Huang, S. K. Lau, H.-w. Tsoi, and K.-y. Yuen, "In silico analysis of orf1ab in coronavirus hku1 genome reveals a unique putative cleavage site of coronavirus hku1 3c-like protease," *Microbiology and Immunology*, vol. 49, no. 10, pp. 899–908, 2005. [Online]. Available: <https://onlinelibrary.wiley.com/doi/abs/10.1111/j.1348-0421.2005.tb03681.x>
- [6] M. Hoffmann, H. Kleine-Weber, S. Schroeder, N. Krüger, T. Herrler, S. Erichsen, T. S. Schiergens, G. Herrler, N.-H. Wu, A. Nitsche, M. A. Müller, C. Drosten, and S. Pöhlmann, "Sars-cov-2 cell entry depends on ace2 and tmprss2 and is blocked by a clinically proven protease inhibitor," *Cell*, vol. 181, no. 2, pp. 271 – 280.e8, 2020. [Online]. Available: <http://www.sciencedirect.com/science/article/pii/S0092867420302294>
- [7] S. Matsuyama, N. Nao, K. Shirato, M. Kawase, S. Saito, I. Takayama, N. Nagata, T. Sekizuka, H. Katoh, F. Kato, M. Sakata, M. Tahara, S. Kutsuna, N. Ohmagari, M. Kuroda, T. Suzuki, T. Kageyama, and M. Takeda, "Enhanced isolation of sars-cov-2 by tmprss2-expressing cells," *Proceedings of the National Academy of Sciences*, vol. 117, no. 13, pp. 7001–7003, 2020. [Online]. Available: <https://www.pnas.org/content/117/13/7001>
- [8] T. H. Bugge, T. M. Antalis, and Q. Wu, "Type ii transmembrane serine proteases," *Journal of Biological Chemistry*, vol. 284, no. 35, pp. 23 177–23 181, 2009. [Online]. Available: <http://www.jbc.org/content/284/35/23177.abstract>
- [9] Y. h. Taguchi and T. Turki, "Neurological disorder drug discovery from gene expression with tensor decomposition," *Current Pharmaceutical Design*, vol. 25, no. 43, pp. 4589–4599, 2019. [Online]. Available: <http://www.eurekaselect.com/node/177329/article>
- [10] J. R. Burdick and D. P. Durand, "Primaquine diphosphate: Inhibition of newcastle disease virus replication," *Antimicrobial Agents and Chemotherapy*, vol. 6, no. 4, pp. 460–464, 1974. [Online]. Available: <https://aac.asm.org/content/6/4/460>
- [11] D. C. CULITA1, R. ALEXANDROVA, L. DYAKOVA, G. MARI-NESECU, L. PATRON, R. KALFIN, and M. ALEXANDROV, "Evaluation of cytotoxic and antiproliferative activity of co(ii), ni(ii), cu(ii) and zn(ii) complexes with meloxicam on virus – transformed tumor cells daniela," *Revista de Chimie*, vol. 63, no. 4, pp. 384–389, 2012.
- [12] H. E. Renis, "Antiviral activity of cytarabine in herpesvirus-infected rats," *Antimicrobial Agents and Chemotherapy*, vol. 4, no. 4, pp. 439–444, 1973. [Online]. Available: <https://aac.asm.org/content/4/4/439>
- [13] K. Ueda, R. Kawabata, T. Irie, Y. Nakai, Y. Tohya, and T. Sakaguchi, "Inactivation of pathogenic viruses by plant-derived tannins: Strong effects of extracts from persimmon (diospyros kaki) on a broad range of viruses," *PLOS ONE*, vol. 8, no. 1, pp. 1–10, 01 2013. [Online]. Available: <https://doi.org/10.1371/journal.pone.0055343>
- [14] R. Li, R. Narita, R. Ouda, C. Kimura, H. Nishimura, M. Yatagai, T. Fujita, and T. Watanabe, "Structure-dependent antiviral activity of catechol derivatives in pyroligneous acid against the encephalomyocarditis virus," *RSC Adv.*, vol. 8, pp. 35 888–35 896, 2018. [Online]. Available: <http://dx.doi.org/10.1039/C8RA07096B>
- [15] P. E. Lobert, D. Hober, A. S. Delannoy, and P. Wattré, "Evidence that neomycin inhibits human cytomegalovirus infection of fibroblasts," *Archives of Virology*, vol. 141, no. 8, pp. 1453–1462, aug 1996. [Online]. Available: <https://doi.org/10.1007/bf01718247>
- [16] H. M. Abuhashish, M. M. Ahmed, D. Sabry, M. M. Khattab, and S. S. Al-Rejaie, "Ace-2/ang1-7/mas cascade mediates ace inhibitor, captopril, protective effects in estrogen-deficient osteoporotic rats," *Biomedicine & Pharmacotherapy*, vol. 92, pp. 58 – 68, 2017. [Online]. Available: <http://www.sciencedirect.com/science/article/pii/S0753332217311873>
- [17] W. Cheng, C. Song, K. M. Anjum, M. Chen, D. Li, H. Zhou, W. Wang, and J. Chen, "Coenzyme q plays opposing roles on bacteria/fungi and viruses in drosophila innate immunity," *International Journal of Immunogenetics*, vol. 38, no. 4, pp. 331–337, 2011. [Online]. Available: <https://onlinelibrary.wiley.com/doi/abs/10.1111/j.1744-313X.2011.01012.x>
- [18] C. M. Finnegan and R. Blumenthal, "Fenretinide inhibits hiv infection by promoting viral endocytosis," *Antiviral Research*, vol. 69, no. 2, pp. 116 – 123, 2006. [Online]. Available: <http://www.sciencedirect.com/science/article/pii/S016635420500241X>
- [19] C. Wu, Y. Liu, Y. Yang, P. Zhang, W. Zhong, Y. Wang, Q. Wang, Y. Xu, M. Li, X. Li, M. Zheng, L. Chen, and H. Li, "Analysis of therapeutic targets for SARS-CoV-2 and discovery of potential drugs by computational methods," *Acta Pharmaceutica Sinica B*, 2020. [Online]. Available: <http://www.sciencedirect.com/science/article/pii/S2211383520302999>
- [20] L. Yi, Z. Li, K. Yuan, X. Qu, J. Chen, G. Wang, H. Zhang, H. Luo, L. Zhu, P. Jiang, L. Chen, Y. Shen, M. Luo, G. Zuo, J. Hu, D. Duan, Y. Nie, X. Shi, W. Wang, Y. Han, T. Li, Y. Liu, M. Ding, H. Deng, and X. Xu, "Small molecules blocking the entry of severe acute respiratory syndrome coronavirus into host cells," *Journal of Virology*, vol. 78, no. 20, pp. 11 334–11 339, 2004. [Online]. Available: <https://jvi.asm.org/content/78/20/11334>
- [21] A. Ubani, F. Agwom, N. Y. Shehu, P. Luka, A. Umera, U. Umar, S. Omale, N. E. Nnadi, and J. C. Aguiyi, "Molecular docking analysis of some phytochemicals on two Sars-Cov-2 targets," *bioRxiv*, 2020. [Online]. Available: <https://www.biorxiv.org/content/early/2020/04/01/2020.03.31.017657>
- [22] C. L. Clouser, S. E. Patterson, and L. M. Mansky, "Exploiting drug repositioning for discovery of a novel hiv combination therapy," *Journal of Virology*, vol. 84, no. 18, pp. 9301–9309, 2010. [Online]. Available: <https://jvi.asm.org/content/84/18/9301>
- [23] K. Fukano, S. Tsukuda, M. Oshima, R. Suzuki, H. Aizaki, M. Ohki, S.-Y. Park, M. Muramatsu, T. Wakita, C. Sureau, Y. Ogasawara, and K. Watashi, "Troglitazone impedes the oligomerization of sodium taurocholate cotransporting polypeptide and entry of hepatitis b virus into hepatocytes," *Frontiers in Microbiology*, vol. 9, p. 3257, 2019. [Online]. Available: <https://www.frontiersin.org/article/10.3389/fmicb.2018.03257>
- [24] O. D. Perez, G. P. Nolan, D. Magda, R. A. Miller, L. A. Herzenberg, and L. A. Herzenberg, "Motexafin gadolinium (gd-tex) selectively induces apoptosis in hiv-1 infected cd4+ t helper cells," *Proceedings of the National Academy of Sciences*, vol. 99, no. 4, pp. 2270–2274, 2002. [Online]. Available: <https://www.pnas.org/content/99/4/2270>
- [25] D. E. Gordon, G. M. Jang, M. Bouhaddou, J. Xu, K. Obernier, M. J. O'Meara, J. Z. Guo, D. L. Swaney, T. A. Tummino, R. Huettnerhain, R. M. Kaake, A. L. Richards, B. Tutuncoglu, H. Foussard, J. Batra, K. Haas, M. Modak, M. Kim, P. Haas, B. J. Polacco, H. Braberg, J. M. Fabius, M. Eckhardt, M. Soucraey, M. J. Bennett, M. Cakir, M. J. McGregor, Q. Li, Z. Z. C. Naing, Y. Zhou, S. Peng, I. T. Kirby, J. E. Melnyk, J. S. Chorb, K. Lou, S. A. Dai, W. Shen, Y. Shi, Z. Zhang, I. Barrio-Hernandez, D. Memon, C. Hernandez-Armenta, C. J. Mathy, T. Perica, K. B. Pilla, S. J. Ganesan, D. J. Saltzberg, R. Ramachandran, L. Liu, S. B. Rosenthal, L. Calviello, S. Venkataramanan, J. Liboy-Lugo, Y. Lin, S. A. Wankowicz, M. Bohn, P. P. Sharp, R. Trenker, J. M. Young, D. A. Caverio, J. Hiatt, T. L. Roth, U. Rathore, A. Subramanian, J. Noack, M. Hubert, F. Roesch, T. Vallet, B. Meyer, K. M. White, L. Miorin, O. S. Rosenberg, K. A. Verba, D. Agard, M. Ott, M. Emerman, D. Ruggero, A. García-Sastre, N. Jura, M. von Zastrow, J. Taunton, A. Ashworth, O. Schwartz, M. Vignuzzi, C. d'Enfert, S. Mukherjee, M. Jacobson, H. S. Malik, D. G. Fujimori, T. Ideker, C. S. Craik, S. Floor, J. S. Fraser, J. Gross, A. Sali, T. Kortemme, P. Beltrao, K. Shokat, B. K. Shoichet, and N. J. Krogan, "A SARS-CoV-2-human protein-protein interaction map reveals drug targets and potential drug-repurposing," *bioRxiv*, 2020. [Online]. Available: <https://www.biorxiv.org/content/early/2020/03/27/2020.03.22.002386>
- [26] Y. Zhou, Y. Hou, J. Shen, Y. Huang, W. Martin, and F. Cheng, "Network-based drug repurposing for novel coronavirus 2019-nCoV/SARS-CoV-2," *Cell Discovery*, vol. 6, no. 1, mar 2020. [Online]. Available: <https://doi.org/10.1038/s41421-020-0153-3>



Y.-H. TAGUCHI received a B.S. degree in physics from the Tokyo Institute of Technology and a Ph.D. degree in physics from the Tokyo Institute of Technology. He is currently a full professor with the Department of Physics, Chuo University, Japan. His works have been published in leading journals such as Physical Review Letters, Bioinformatics, and Scientific Reports. His research interests include bioinformatics, machine learning, and nonlinear physics. He is also an editorial board member of Frontiers in Genetics:RNA, PloS ONE, BMC Medical Genomics, Medicine (Lippincott Williams & Wilkins journal), BMC Research Notes, non-coding RNA (MDPI), and IPSJ Transaction on Bioinformatics.



TURKI TURKI received a B.S. in computer science from King Abdulaziz University, an M.S. in computer science from NYU.POLY, and a Ph.D. in computer science from the New Jersey Institute of Technology. He is currently an assistant professor with the Department of Computer Science, King Abdulaziz University, Saudi Arabia. His research interests include artificial intelligence, machine learning, deep learning, data mining, data science, big data analytics, and bioinformatics. His research has been accepted and published in journals such as Frontiers in Genetics, BMC Genomics, BMC Systems Biology, Expert Systems with Applications, Computers in Biology and Medicine, and Current Pharmaceutical Design. He was awarded several distinction awards from the Deanship of Scientific Research at King Abdulaziz University. He is supported by King Abdulaziz University and is currently working on several biomedicine related projects. Dr. Turki has served on the program committees of several international conferences. Additionally, he is an editorial board member of Sustainable Computing: Informatics and Systems and Computers in Biology and Medicine.